Chapter 11
The Subsiding Macrotidal Barrier Estuarine System of the Eastern Amazon Coast, Northern Brazil

Pedro W. M. Souza-Filho, Guilherme C. Lessa, Marcelo C. L. Cohen, Francisco R. Costa and Ruben J. Lara

11.1 Introduction

The northern Brazilian coast is 1,200 km long and encompasses two geo-morphologic world records: the largest mangrove system (Souza Filho 2005) and the gorge of the largest river in length, water and sediment discharge, the Amazon. Dominguez (Chap. 2, this volume) classifies the northern Brazilian coast in two sectors: i) the tide-muddy dominated coast of Amapá-Guianas in the west, and ii) the tide-dominated mangrove coast of Pará-Maranhão in the east (Fig. 11.1). The tide-dominated eastern sector is 480 km long with 7,600 km^2 of continuous mangrove forests (Souza Filho 2005), almost twice as large as the Sunderbands in India-Bangladesh (Kjerfve et al. 2002). The coastline is extremely irregular and jagged, harboring 23 estuaries and 30 catchment areas that drain an area of 330 mil km^2 (Martins et al. 2007). The Quaternary coastal history of this region has been controlled by the structural-sedimentary evolution of Pará-Maranhão, Bragança-Viseu and São Luís Equatorial coastal basins (Souza Filho 2000). The geological control coupled with Quaternary sea-level changes, large fluvial sediment supply and the reworking of relict sediments on the continental shelf have controlled the Amazon coastal evolution.

The purpose of this chapter is to provide an overall characterization of the coastal geomorphology of the tide-dominated mangrove coast of the northeastern Pará State, on the Amazon mangrove coast (Fig. 11.1), with special attention to the barrier-estuarine system of Caeté (Fig. 11.2), that will be used as a proxy for the morpho-sedimentary evolution of this coastal sector.
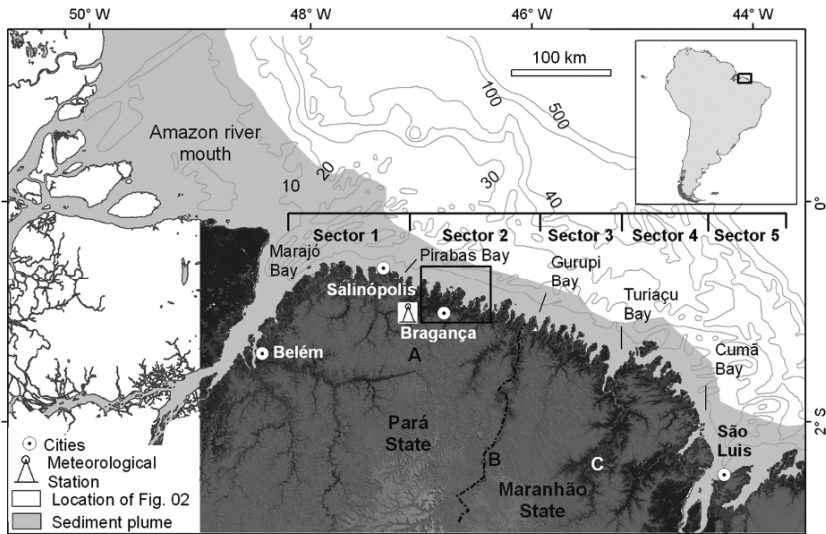
Fig. 11.1 The northern macrotidal Brazilian coast and location of the study area in the northeast of the State of Pará (*black rectangle*) with the distribution of coastal plateaus (*light gray tones*) and wetlands (*dark grayish tones*). Five different coastal sectors are identified (see text). The image is a digital elevation model processed from SRTM data

11.2 Regional Setting

11.2.1 Structural Setting

The northern Brazilian continental margin is part of a transform margin established in the Early Cretaceous (Campos et al. 1974), with its tectonic setting associated with the NW-SE Romanche fracture zone characterized by horst and graben structures (Gorini and Bryan 1976). In the study area, two grabens lying inland from the shoreline form the São Luís and Bragança-Viseu basins, delimited in the south by the Ferrer-Urbano Santos arch (Aranha et al. 1990) (Fig. 11.3).
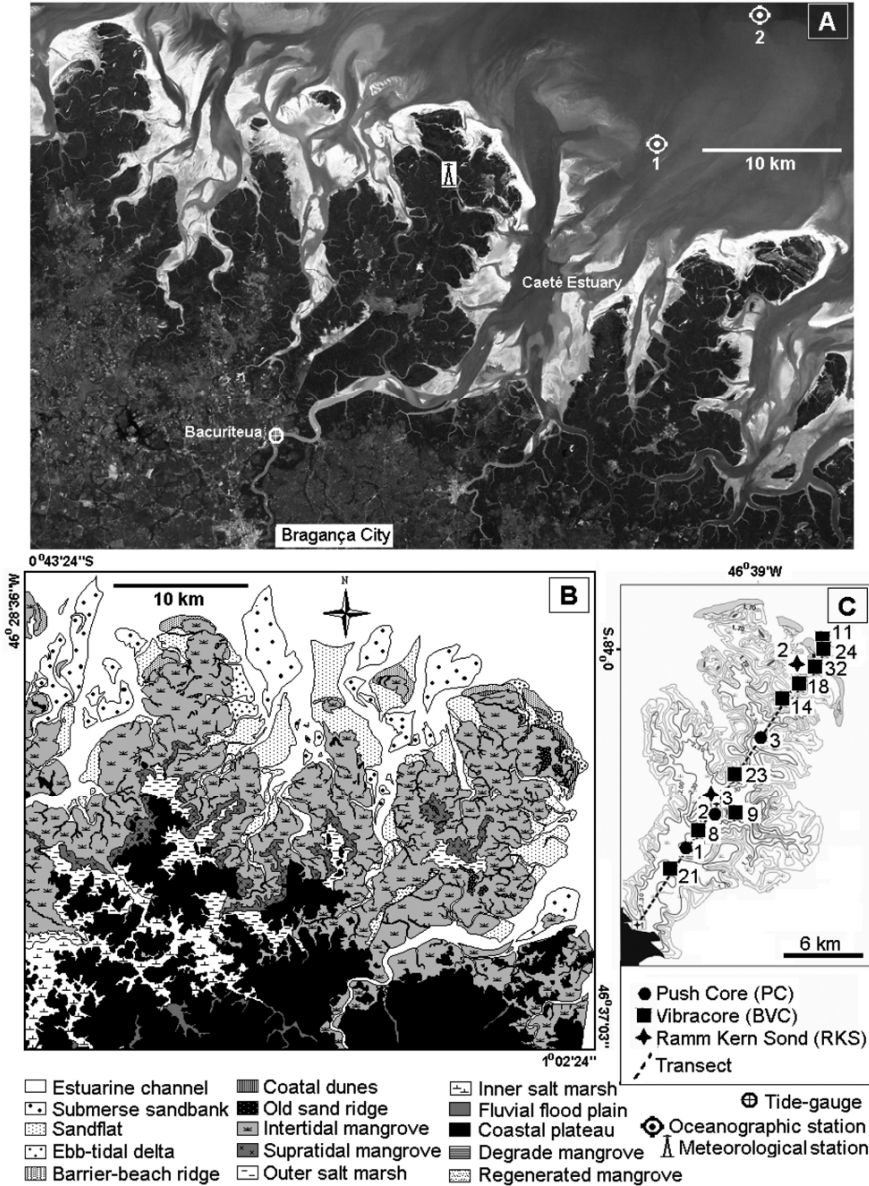
Fig. 11.2 (**A**) Landsat TM images (Band 3) showing the spatial distribution of sand flats (*light gray tones*) and mangroves and marshes (*dark gray tones*). The meteorological station is positioned on the left margin of Caeté estuary and numbers 1 and 2 indicate the position of oceanographic stations. (**B**) Map of the coastal environments in the area (Souza Filho and Paradella 2005). (**C**) Topographic map with coring sites (Cohen et al. 2005)

Souza Filho (2005) divided the area in five sectors (Fig. 11.1) based on its geomorphological characteristics. In Sector 1, the coastal plateaus reach the shoreline and the coastal plain is narrow. In sectors 2, 3 and 4, corresponding to the study area, the coastal plain widens as the coastal plateaus recede southward. Sector 2 extends between the Pirabas and Gurupi bays and abuts a small coastal horst delimiting the northern side of Bragança-Viseu basin (Fig. 11.3). The costal plain widens eastward, following an inactive cliff 1 m to 3 m in height. Results from ground penetrating radar (GPR) profiles across the paleo-cliff revealed downward displaced faulted blocks (Fig. 11.4) bordering the northern side of the horst (Rossetti 2003). Continuous subsidence has created space to accommodate sediments since the Middle Miocene (Rossetti 2003). Sector 3, extending from Gurupi to Turiaçu Bay, is set over the Gurupi horst, a stratigraphic window where Proterozoic rocks outcrop near the coast (Gorayeb et al. 1999; Klein et al. 2002). Here the coastal plain, limited by the paleo-cliff in the south, reaches its maximum width (40 km), forming a much more jagged coast. Sector 4, between the Turiaçu and Cumã bays, harbors the narrowest coastal plains, that reach a maximum width of 26 km. Akin to Sector 2, Sector 4 abuts a coastal horst (Aranha et al. 1990; Ferreira Jr. et al. 1996) delimiting the São Luís basin to the north (Fig. 11.4). In the eastern side of this sector, Costa et al. (2002) and Ferreira Jr. et al. (1996) presented sets of E-W, ENE-WSW strike-slip faults linked to NW-SE and NNW-SSE normal faults (Fig. 11.4b).

The paleo-cliff that limits the coastal plain along Sectors 2, 3 and 4 is apparently a normal active fault associated with a downward movement of the coastal plain (Souza Filho and El-Robrini 2000). Activation of this fault line appears to be related to a NW-SE extensional stress and flexural bending of the lithosphere caused by sediment loading on the Amazon continental shelf and erosion in the adjacent coastal plain (Driskoll and Karner 1994).

11.2.2 Continental Shelf Morphology and Sedimentology

The shelf off the Amazon River is more than 300 km wide and gently inclined, with an overall gradient of 1:2,240 until the shelf break at 100 m deep (Milliman 1979) (Fig. 11.5). The outer shelf is dominated by carbonate sedimentation (Fig. 11.4a), both in the form of sand and reefs that have been dated at 17,000 years BP (Milliman and Barreto 1975). The inner shelf initiates approximately at the 20 m isobath (15 km away from the coast along the northeast of Pará State), where transgressive siliciclastic marine sands start to occur (Fig. 11.4a). The majority of the sand is composed of well sorted clear quartz (Zembruscki et al. 1971) and sug-

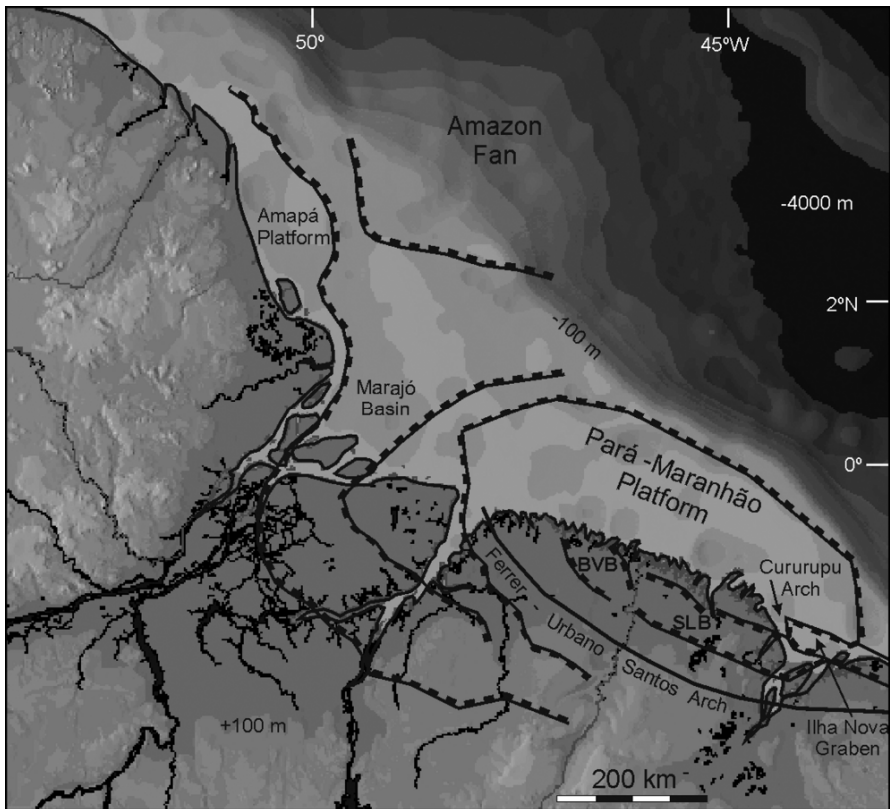gests a marine origin. Relict sedimentation associated with riverine sands occurs in a few patches.

Fig. 11.3 Physiographic and structural framework map of the northern Brazilian coast (modified from Gorini and Bryan 1976). BVB refers to Bragança-Viseu Basin and SLB refers to São Luiz Basin

The inner shelf is topographically characterized by elongated platforms up to 70 km long and 7 km wide, oriented normal to the coast and associated with paleo-drainage channels that today have a topographic relief between 8 m to 20 m deep (Zembruscki et al. 1971). These valleys lend a jigsaw character to the contour lines, and are more prominent in the east (Fig. 11.5) near the coast of Maranhão, where larger estuaries (associated with larger tidal prisms) exist. Superimposed over the elongated platforms well-developed dunes occur, 3 to 4 m high, symmetrical in the nearshore and asymmetrical (oriented to the west) on the middle shelf (Zembruscki et al. 1971). West of Marajó Bay, the whole shelf is covered with a mud wedge (Fig. 11.4a) more than 20 m thick that downlaps the transgressive

siliciclastic sands down to approximately the 65 m isobath (Milliman 1979).

11.2.3 Climate

The climate in the Amazon coast is governed by seasonal changes in the position of the Inter-tropical Convergence Zone (ITCZ) and instability lines. Climatologically, the latitudinal position of the ITCZ is around 14° N in August and September, and around 2° S in March and April. Mean annual rainfall along the studied coast increases westward, from 2250 mm to 2650 mm at Salinas (Fig. 11.6). A thirty year record of the Traquateua meteorological station, 15 km west from Bragança (see location in Fig. 11.1), indicates that the annual mean precipitation ranges from 2300 mm to 2800 mm (Moraes et al. 2005). The wet season is well defined between January and April, when 73% of the annual precipitation occurs. The dry season occurs between September and November with near-to-zero mean precipitation.

River discharges vary accordingly to the catchment size, which range from 508 km^2 to 35,200 km^2 within the study area (Fig. 11.7). The monthly-mean discharge for three characteristic catchment sizes (Gurupi = 35,200 km^2, Turiaçu = 13,032 km^2 and Caeté = 1,546 km^2) is given in Fig. 11.8. Highest discharges occur in April, reaching 1277 m^3/s at Gurupi River and 47 m^3/s at Caeté. Maximum river discharges have been calculated at 2478 m^3/s, 1393 m^3/s m and 257 m^3/s for the Gurupi, Turiaçu and Caeté rivers, respectively.

Based on wind data (January 2003 to May 2005) from a meteorological station located on the Caeté peninsula (see location in Fig. 11.2), the easterly trade winds blow throughout the year, with average velocities between 2 m/s and 4 m/s (Fig. 11.9a). Seasonal variations, however, occur due to the proximity of the ICTZ between January and April. Whereas easterly winds account for almost 70% of the record in the dry season, with average velocities between 4 m/s and 6 m/s (Fig. 11.9b). Strongest winds occur in September, with a maximum speed of about 10 m/s.

11.2.4 Oceanography

The tides in the region are semidiurnal, with mean spring tide ranges $(2(M_2+S_2))$ around 3.3 m on the inner shelf (Brazilian Hydrographic Authority Data Bank), but apparently undergo amplification inside the
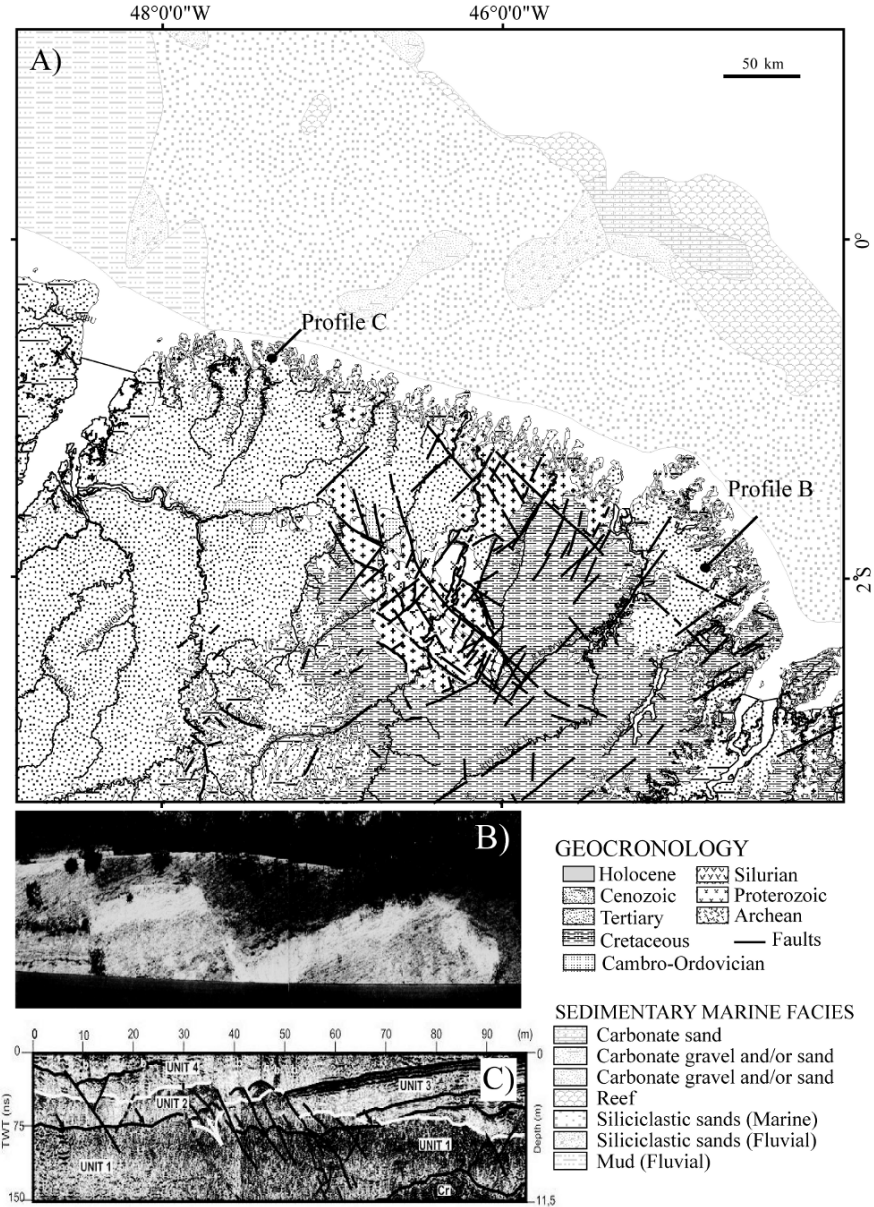
Fig. 11.4 (A) Geologic map of the study area (CPRM 2001) with stratigraphy **(B)** and GPR **(C)** evidence of recent tectonic movements. The picture **(B)** is an outcrop showing rotational slips (direction NW-SE) (Ferreira Jr. et al. 1996), whereas the GPR profile (Rossetti 2003) shows Miocene (*below white line*) deposits disrupted by faults (*inclined black lines*)
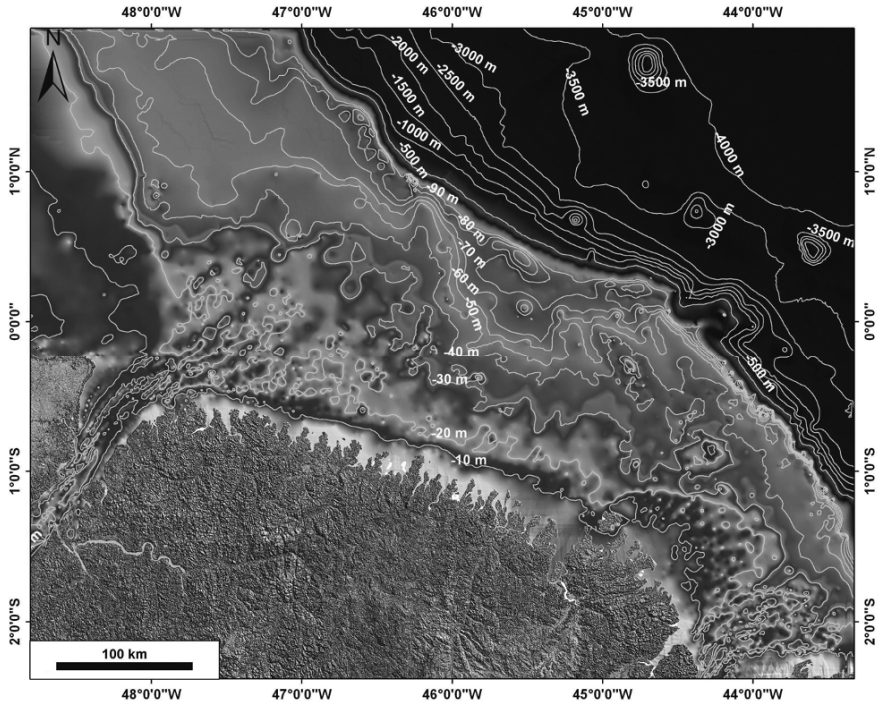
Fig. 11.5 A bathymetric model with the isobaths on the continental shelf. Notice the jigsaw character of the inner shelf, with valleys that are more prominent on the eastern side

estuaries. A one year long (June 2003–June 2004) tidal record at Bacuriteua, 20 km upstream from the mouth of Caeté estuary (location in Fig. 11.2), shows that tide range varies from a minimum of 1.76 m to a maximum of 5.37 m. Seasonal sea-level variations can be more than 20 cm in Bacuriteua, with higher sea levels in April (period of highest fluvial discharges) and September (time of the strongest E-NE winds). Mean tidal range at Ajuruteua Beach measures around 4 m in a semi-diurnal cycle, although this range during the spring tides is locally as high as 5 m (Souza Filho et al. 2003). Thus, during the spring tides, large areas of the low land are inundated by water as a result of both high rainfall-runoff rates and tidal processes. The tide wave is asymmetrical (shorter rising tides), but displays a sharp decrease of rising rates about 2 hours before high spring tides, when extensive intertidal areas (vegetated or not) become inundated.

In similarity to other macrotidal estuaries, this pattern of tidal asymmetry is morphodynamic in character and can drive stronger ebb flows (Lessa 2000). Close to Bacuriteua, faster ebb-flows reach a velocity maximum of

1.5 ms^{-1} at the surface. Flood flows, on the other hand, tend to be faster at the mouth (maximum surface values also about 1.5 ms^{-1}) where the mangrove area is limited (Susane Rabelo, personal communication).

According to data collected by the Brazilian Navy (DHN 1962), the average current velocity at the rising tide on the inner-shelf (NE-SW to E-W flows) is 0.97 m/s (maximum of 1.43 m/s in June-July), whereas the falling tide velocities (W-E to SW-NE flows) vary from 1.07 to 1.11 m/s. Cavalcante et al. (2005) monitored the velocity of the water column (with an ADCP) at two stations (see Fig. 11.2 for location) on the inner-shelf in March and April 2003. The stations were located 5 km and 25 km from the coastline, at water depths of 20 m and 35 m respectively. Measurements were undertaken for 25 hours both on neap and spring tides. Maximum current magnitudes (at about 5 m of depth in the two stations) reached 0.87 m/s at station #1 and 1.0 m/s at station #2, whereas the vertical mean magnitudes were around 0.50 m/s in both stations. Current directions were parallel to the coastline at station #2, but normal to the coastline at station #1, aligned with the estuary mouth. In the latter, as a consequence of large fluvial discharges, the water column in the inner shelf can be partially mixed in the winter. Cavalcante et al. (2005) report the existence of a well defined halocline in both stations, situated on average at 3 m and 6 m depth in the closest and farthest stations respectively (Fig. 11.10). At the shoreline NE waves can reach 2 m in height (CPTEC/INPE 2004). Maximum flood-current velocities (0.87 m/s directed to the estuary) were stronger than ebb (0.70 m/s), and point to potential sediment transport towards the estuary.

11.3 Data Sources

Figure 11.2c shows the location of fifteen sediment cores obtained from the study area, all of them approximately aligned with a cross-normal transect to the coastline. Out of the fifteen cores, there are nine 6 m long vibracores (BVC) taken from the intertidal area (see position in Fig. 11.2c), whose analysis were published by Souza Filho and El-Robrini (1998) (exception made to BVC-09). Three other cores were collected with a percussion-core (PC) and their results published by Behling et al. (2001).

More recently we have obtained three cores (RKS-1, RKS-2 and RKS-3) with a Ramm Kern Sonde set with a soil recovery probe. Coring was executed close to the boundary between the coastal plateau and the mangrove area (RKS-1), on a chenier ridge (RKS-2) and on a marsh surface
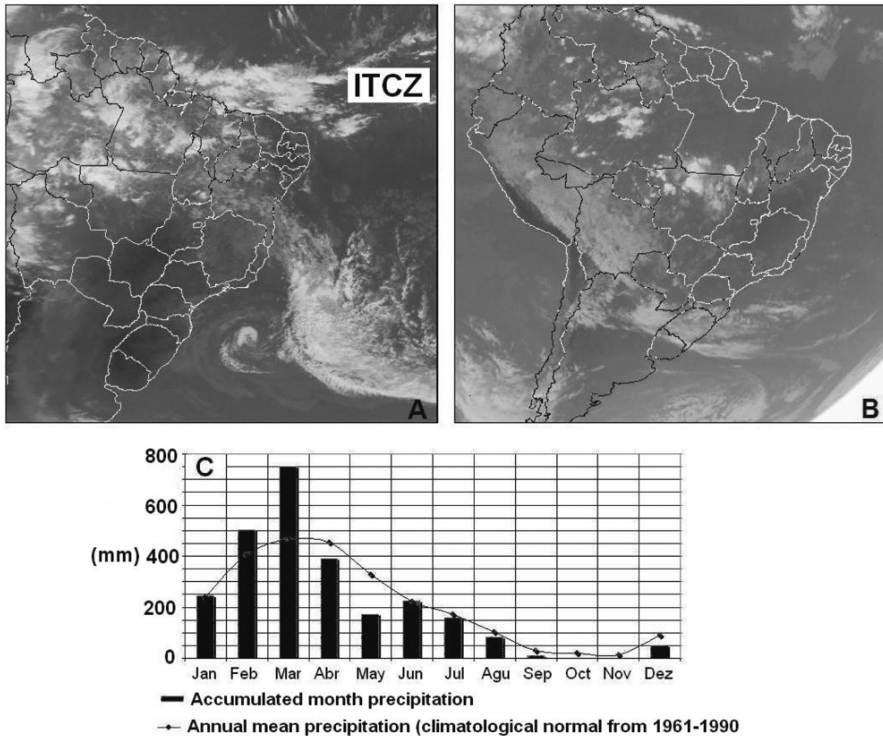
Fig. 11.6 GOES satelite image showing the position of the ITCZ over South American on March 03, 2004 (**A**) and August 25, 2004 (**B**) (Source: CPTEC/INPE). (**C**) - Distribution of the monthly-mean precipitation at Traquateua Station (Source: INMET)

(RKS-3), reaching 19.10, 17.60, and 17.80 m in depth, respectively. Souza Filho et al. (2006) have used this dataset, but with no description of the cores. Radiocarbon dates have been performed on 11 samples obtained from 6 cores (Koch et al. 2003; Behling et al. 2001)**.** Ages range from Modern to 5,916 cal yrs BP. Results of pollen analyses presented by Behling et al. (2001) were also used to help with the recognition and interpretation of sedimentary facies.

On the basis of morphology, lithology, sedimentary structures, texture, color, pollen content, elevation and contact, 10 sedimentary facies overlaying the Miocene substrate were identified in the barrier and the estuarine intertidal zone. Figure 11.11 presents the lithology and sedimentary structures described in the BVC vibracores and PC percussion-cores, while Figs. 11.12, 11.13 and 11.14 illustrate the RKS #1, RKS #3, and RKS #2, respectively.

The substrates for the Quaternary sedimentation include the Miocene siliciclastic sands and muds of Barreiras Formation (Rossetti 2001) at the bottom (17 m in depth) of core RKS #1 (Fig. 11.12), and the Miocene carbonates of the Pirabas Formation (Rossetti 2001) at the base (10.5 m in depth) of the RKS #3 (Fig. 11.13). From the oldest to the youngest, the facies are:
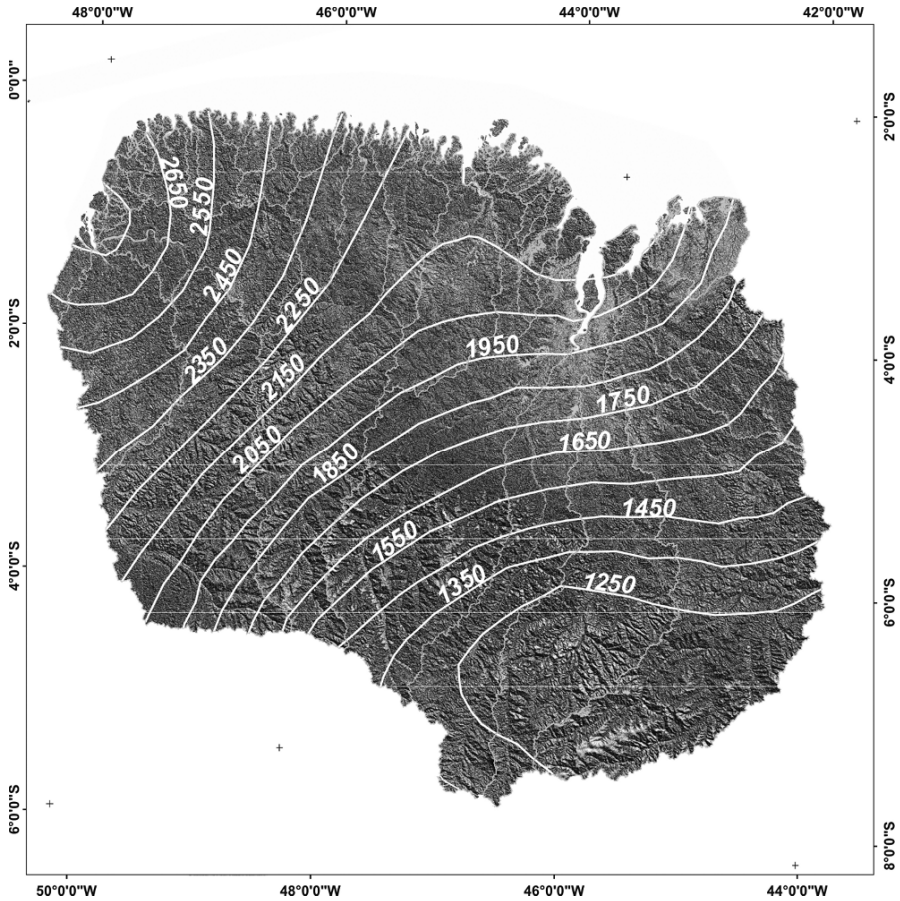

Fig. 11.7 Contours of the catchment areas (*in light gray*) and isohyets (mm/year - *white lines*) within the study area
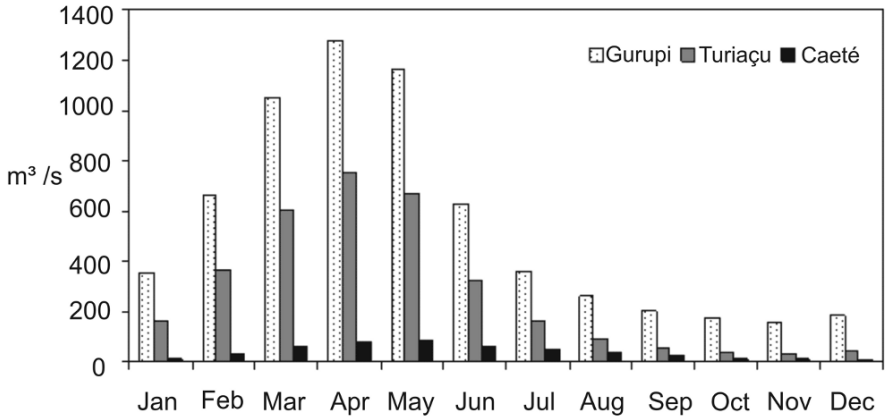
Fig. 11.8 Monthly-mean discharges for the Gurupi, Turiaçu and Caeté rivers (see Fig. 11.2 for location), associated with a large, medium and small catchment area. The discharge time series extended from 1964 to 1971 in both stations in the Caeté River and from 1972 to 1999 in the Gurupi and Turiaçu rivers
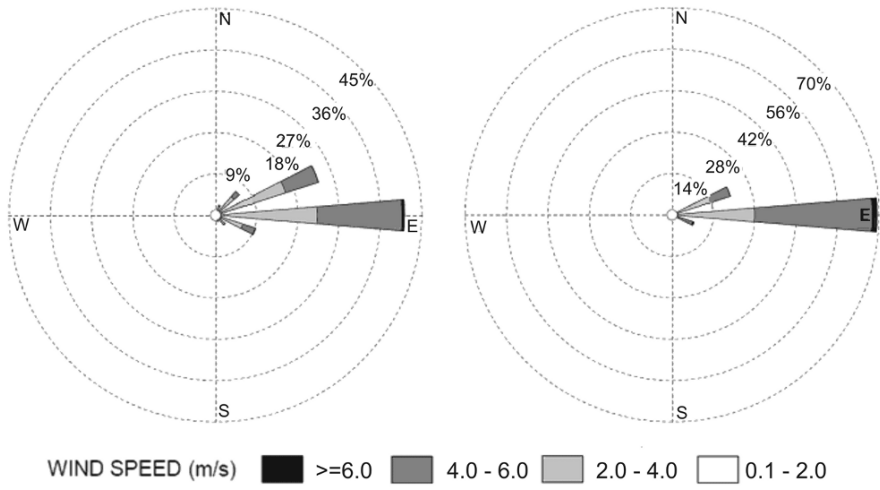

WIND SPEED (m/s)   ■ >=6.0   ■ 4.0 - 6.0   ☐ 2.0 - 4.0   ☐ 0.1 - 2.0

Fig. 11.9 Average wind velocity distribution for the rainy (left) and dry (right) seasons in Traquateua (see location in Fig. 11.2)
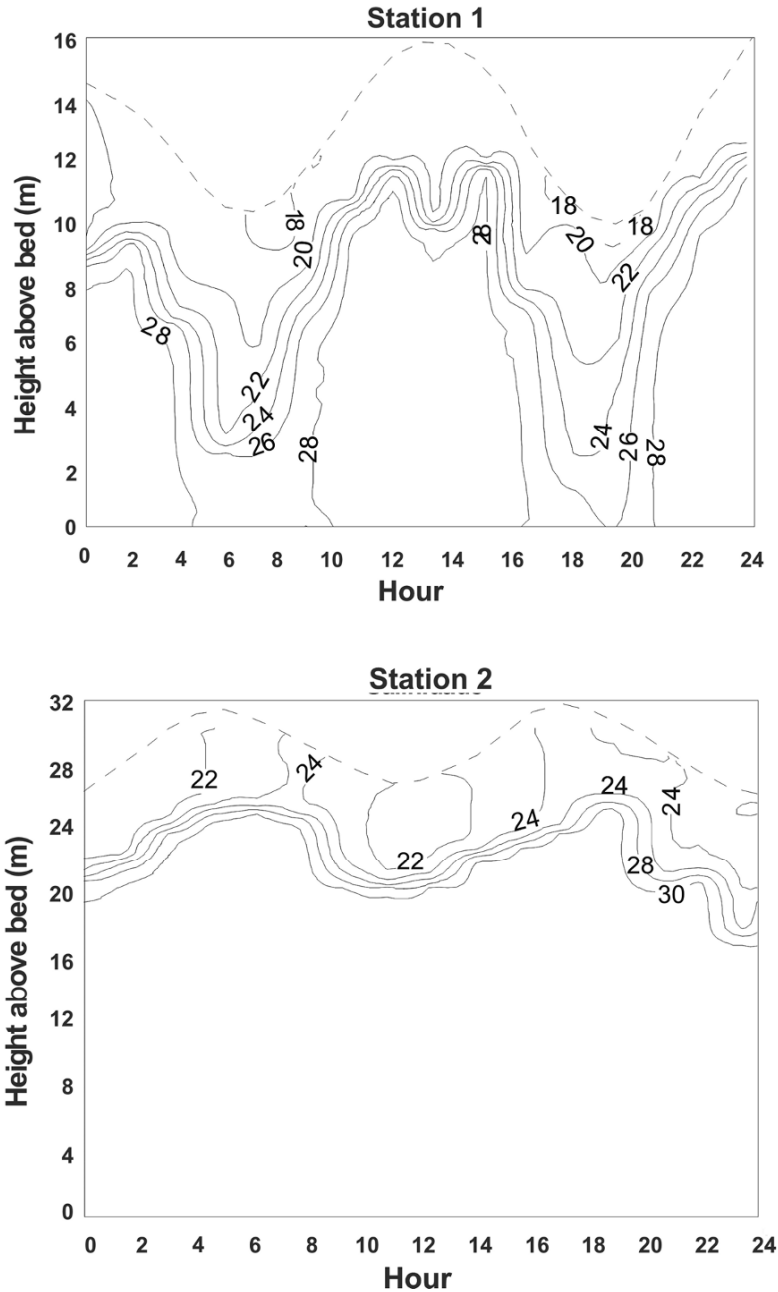
Fig. 11.10 Variation of the salinity field along two tidal cycles on the *inner* shelf fronting the Caeté estuary. Stations #1 and #2 are 5 and 25 km off the coastline, respectively (see Fig. 11.2 for location) (after Cavalcante et al. 2005)
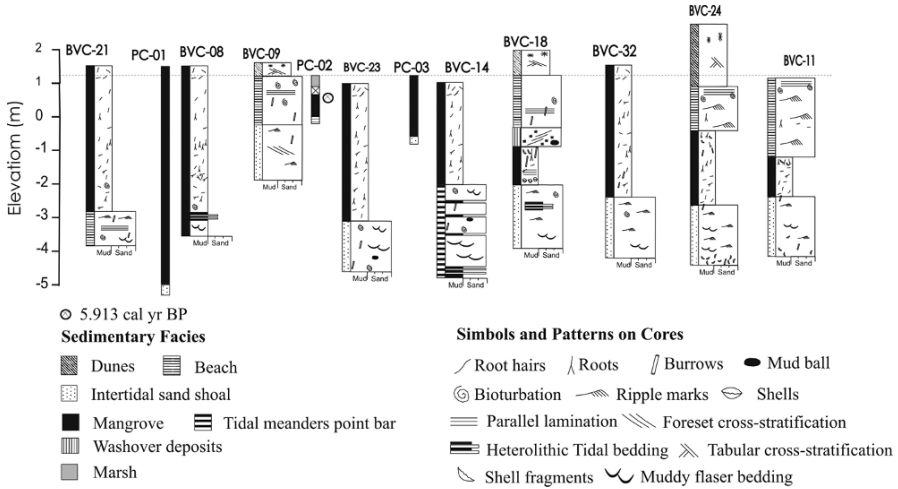
Fig. 11.11 Lithology and sedimentary structures described in the vibracores (BVC) and percussion-cores (PC) along the Bragança Peninsula. See location in Fig. 11.2C. 0 m = MSL

(1) Pre-Holocene fluvial channel: composed of poorly-sorted, very coarse quartz sand to gravel and light gray in color. This facies was only found in RKS #1 with a thickness of 1.5 m, at a depth of 15.6 m, and appears to fill in an incised paleo-valley. The environment of deposition (fluvial channel landward of the bayline) was suggested based on the lithological similarity between this facies and the present fluvial deposits. (Fig. 11.12).

(2) Transgressive-mud facies: composition of this facies is characterized by more than 70 % of fine sediments (<0.062 mm), with a small percentage of very fine quartz sand and shell fragments. The transgressive-mud facies was identified in cores RKS #2 and RKS #3 resting on the substrate (Figs. 11.14 and 11.13, respectively) and overlaid by the subtidal sand-flat and aeolian sand facies. This facies shallows landwards, from ~ -15.8 m in RKS #2 to ~ -10 m in RKS #3.

(3) Tidal meanders facies: is composed of laminations of white, fine quartz sand and gray-greenish mud, mostly bioturbated and with root fragments. It was found in core RKS #1 between −10 to −15 m (Fig. 11.11) overlying the Pre-Holocene fluvial channel facies, in abrupt contact, and underlying the aeolian sand facies.

(4) Aeolian sand facies: this facies is composed predominantly of light-gray, fine-quartz sand beds, mostly bioturbed and intercalated with fine-mud beds that were radiocarbon dated at 37,110 ± 310 yrs BP (Fig. 11. 12). Parallel sand laminations (highlighted by organic matter) are the most

frequent sedimentary structures. The contact between the dune and inter-dune subfacies and the underlying tidal meandering facies is abrupt and marked by a discordance, while the contact with the overlying intertidal shoal facies is likely to be erosive, defined by gravelly coarse sands. According to Koch et al. (2003), analyses of organic compounds in the sediments suggest fluvial deposition, while biomarker distributions reveal the presence of herbal species. However, based on stratigraphic analysis this deposit can be associated to fresh water lakes in the interdune zones. The dune subfacies represents vegetated foredunes, composed by well-sorted very fine quartz sands with few shell fragments, with oxidation features and massive and tabular cross-bed sets bioturbated by roots and worm tubes. This facies overlies the tidal meander facies (RKS#1, Fig. 11.12) and transgressive mud facies (RKS#3, Fig. 11.13), with thicknesses varying between 3 to 5.5 m.

(5) Subtidal sand-flat facies: is composed of rounded and well-sorted fine quartz sands with shell fragments. The sediments are light-gray in color with a greenish hue due to different degrees of mud content. Characteristic sedimentary structures are cross-bedding, flaser and bioturbation, which lends a mottled structure to the deposit. The contact between this facies and the underlying transgressive mud facies is abrupt, whereas the contact with the overlying barrier-island facies is marked by an erosion surface where medium to coarse sand, rich in shell fragments, accumulates (Fig. 11.13). The presence of marine organisms associated with sedimentary structures is an indication that the deposition of this facies, although driven by tidal processes inside the estuary, was also influenced by marine conditions.

(6) Intertidal sand shoal facies: is comprised of a very fine, well-sorted, rounded, white to very light-gray quartz sands, with sparse concentration of shell fragments and pieces of mangrove wood. The main sedimentary structures are bioturbated flaser bedding and small scale cross-stratification associated to ripple marks. This facies can be subdivided into an upper and lower section based on the sedimentary structures (Fig. 11.4). While the lower section is mostly characterized by a profusion of flaser beddings and cross-stratification, a more significant amount of shells and shell fragments are common in the upper section. The lower and upper contacts of this facies are commonly gradational, overlying upper-flow regime sand flats, transgressive muds and subtidal sand-bar facies, and underlying old beach-ridges and mudflats as well as recent mangroves. This facies is the thickest sedimentary unit, forming a wedge that thickens from 6 m at RKS #1 (landward side, Fig. 11.13) to 10 m at RKS #2 (seaward side, Fig. 11.14).

(7) Barrier-island facies: is composed of a fine, well-sorted, rounded, white and brownish (iron stained) quartz sands with sparse shell fragments.

It is generally made of three subfacies, which are beach, dune and washover facies. Three generations of barrier-islands were recognized in the plain, as follows:
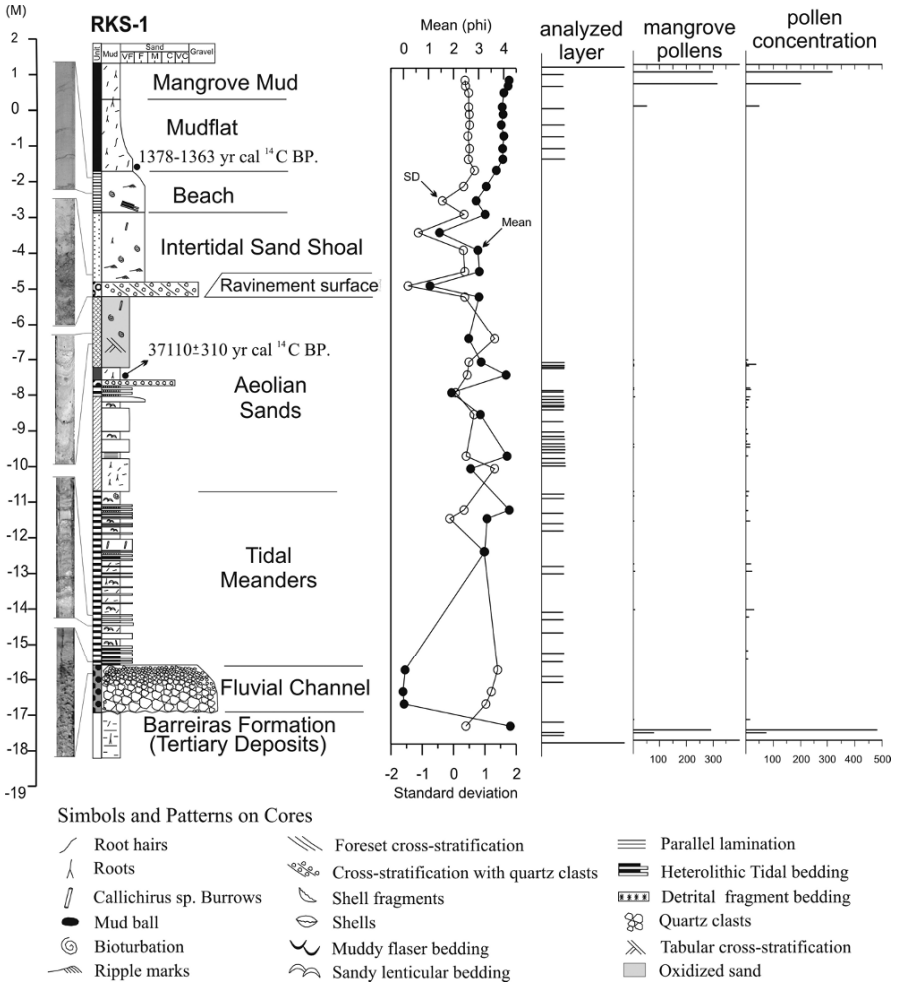

Fig. 11.12 Sedimentary core RKS #1 showing the vertical succession of facies, grain size and pollen occurrence. 0 m = MSL
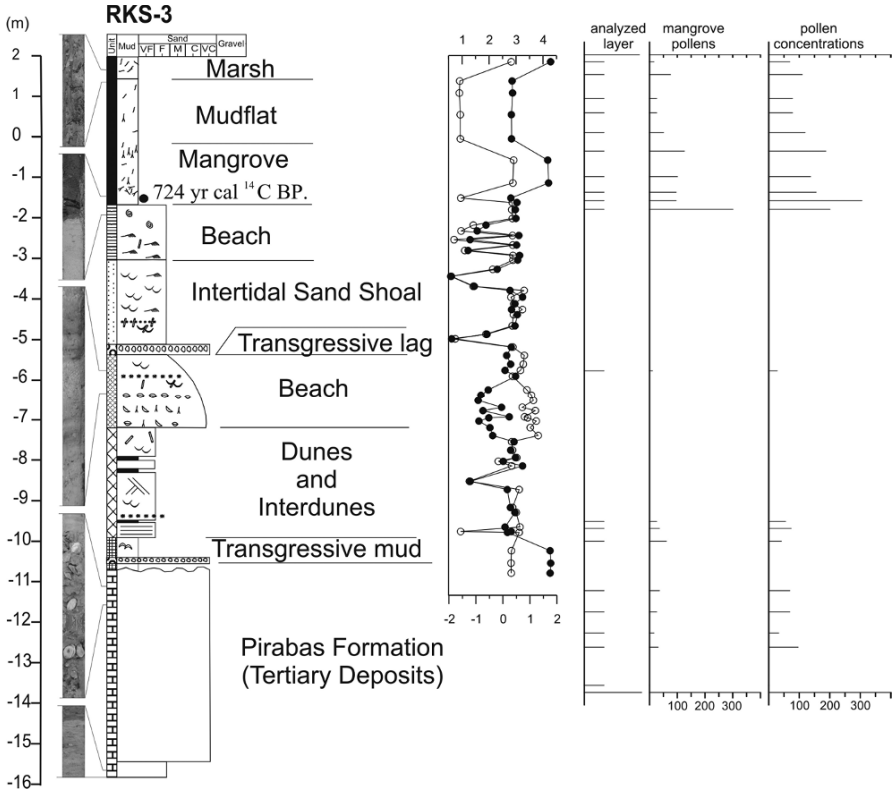
Fig. 11.13 Sedimentary core RKS # 3 showing the vertical succession of facies, grain size and pollen occurrence. 0 m = MSL

-First barrier island: represents the oldest barrier that outcrops along the Bragança-Ajuruteua road, 12 km landward from the present shoreline. Its beach subfacies was recognized from parallel lamination and bioturbation, while an aeolian dune subfacies was indicated by climbing laminations and preserved surface morphology. This barrier was cored by RKS #2 (from ~ +1.4 to –1.5 m; Fig. 11.14) and BVC #9 (from +1.4 to -0,5 m in elevation; Fig. 11.11). It overlies the intertidal shoal facies and underlies mangrove mud facies. The contact between the barrier and mangrove facies was radiocarbon dated (UtC-8737) at 5,913 cal yrs BP.

-Second barrier island: This barrier crops out 2.5 km landward of the present shoreline, and was cored by RKS #2 (from surface to 1.2 m in elevation; Fig. 11.14) and BVC #18 (Fig. 11.11). It overlies mangrove mud facies radiocarbon dated at 2,800 cal yrs BP. Its lower contact is abrupt, truncating animal burrows filled with fine sands. This facies can be subdivided in three sub-facies: i) dune facies, composed of very fine, white sand with large tabular cross-stratification, with the original morphology still

preserved; (ii) beach facies, composed of iron-stained fine sands with massive and mottled structures ascribed to bioturbation; and (iii) washover facies, distinguished by cross-stratification with foresets dipping 23º landward.
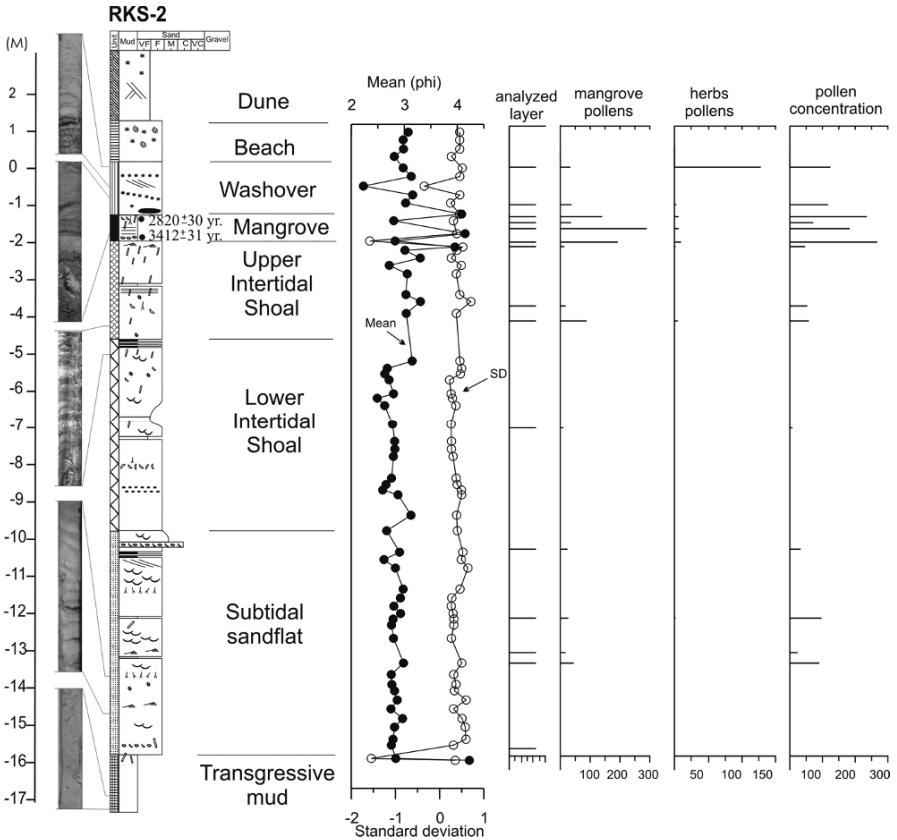

Fig. 11.14 Sedimentary core RKS # 2 showing the vertical succession of facies, grain size and pollen occurrence. 0 m = MSL

-Third barrier island: given its pristine condition, it was possible to differentiate five sub-facies: (i) vegetated and mobile coastal dunes with climbing and tabular cross-stratification; (ii) high intertidal zone with inclined plane-parallel lamina defined by an intercalation of quartz and heavy minerals; (iii) mid-intertidal zone with plane-parallel sedimentary structures; (iv) low intertidal zone with low angle cross-stratification suggesting shallow alongshore channels with, and (v) subtidal zone composed

of mixed sand-mud sediments densely bioturbed by burrows of *Callichirus* sp. and other crustaceans (Souza Filho et al. 2003).

Characteristic elevations for the third barrier island are +7 m (on the dunes), +2.8 m (on the beach scarp) and –1 m (in the bottom of BVC #11, Fig. 11.11). Mangrove mud facies underlie this island and is presently on-lapping dune deposits in its rear. The lower contact is abrupt, and is interpreted as a wave-ravinement surface (BVC #11; Fig. 11.11). Figure 11.15 shows the present morphology of the third barrier-island.

(8) Mudflat facies: is composed of a soft, dark gray and organic-rich mud, with mean grain size commonly about 4.005 ϕ. Lenticular beddings are common. This unit is restricted to RKS #1 from 0.45 to 3.0 m in elevation (Fig. 11.12), where mangrove pollens were not found. This unit is interpreted as a progradational mudflat that overlies the intertidal sand shoal facies with the contact characterized by an abrupt textural change, from very fine sand to mud.

(9) Mangrove mud facies: a soft, dark gray, highly organic mud, found at the top of most of the cores (Fig. 11.11). The maximum elevation of this facies is about +2.4 m above the mean sea-level, and the minimum elevation is around -4.5 m. Its thickness increases seaward, from 1.7 m (RKS #3, Fig. 11.13) to 5-6 m (PC #01, Fig. 11.11). The mangrove mud overlies the mudflat, intertidal sand shoal and 1st transgressive barrier island facies, and is interpreted as a progradational unit, with radiocarbon ages younger than 2,119-1,994 cal yrs BP.

(10) Marsh mud facies: composed of hard, dark gray and organic mud. The top of this facies is marked by mud cracks and salt accumulation during the dry season, defining a sub-aerial exposure surface. The contact between marsh mud facies and the underlying mangrove mud facies is defined by a significant decrease in *Rhizophora, Avicennia* and *Laguncularia* pollens and an increase of *Poaceae, Cyperaceae, Acanthaceae, Amaranthaceae-chenopodiaceae, Alternanthera, Asteraceae-Asterioideae, Asteraceae-Cichorioideae, Borreria* and *Spermacoceae* pollens towards the top. This contact was radiocarbon dated (UtC-8724) at 483-434 cal yrs BP. (Behling et al. 2001). The unit is distributed over the highest areas of the plain (+2.6 m above mean sea-level) densely covered by grassland. Based on the pollen record, this is 0.5 m in thick in RKS #3 (Fig. 11.13).
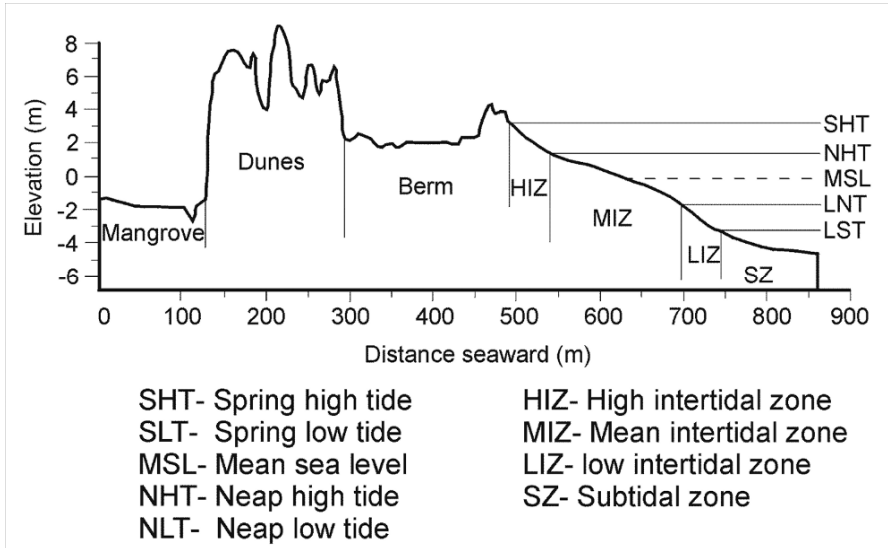
Fig. 11.15 Morphologic details of the third transgressive barrier-island in the Aju-ruteua macrotidal sandy beach (Souza Filho et al. 2003). 0 m = MSL

11.4 Evolution of the Barrier-Estuarine System

Figure 11.16 shows the cross-normal morphostratigraphic profile between the coastal plateau and the third barrier-island. The basement depth below the Quaternary deposits was reached at around 17, 10.5 and 17.3 m, in RKS-1, RKS-3, and RKS-2, respectively (Figs. 11.12, 11.13 and 11.14). Based on the RKS vibracores, the basement surface shows a steep paleo-cliff carved in the Barreiras formation in direct contact with Quaternary deposits (Fig. 11.16). At the base of the paleo-cliff a wide undulated Ter-tiary surface occurs, composed of carbonaceous deposits of the Pirabas Formation (RKS-3) and siliciclastic sediments of the Barreiras Formation (RKS-1).

The base of the Quaternary sedimentation is represented by the Pre-Holocene fluvial sand and gravel facies deposited in a fluvial channel sec-tion carved into the Tertiary deposits (Fig. 11.16). The incised valley would be older than the fluvial deposits, which may rest on a sequence limit and harbor an initial inundation surface. This initial inundation sur-face may also be represented by the contact between the transgressive mud facies and the Miocene substrate (Facies 2, RKS #2 and RKS #3). The de-

position of this facies followed the inundation of the lowlands with fringing marsh and mangrove muds, and suggests the presence of a barrier
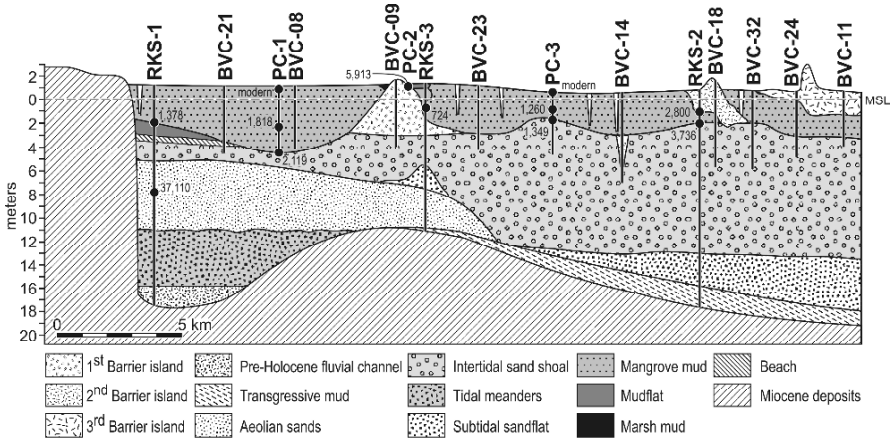

Fig. 11.16 Cross-normal morphostratigraphic profile along the Bragança coastal plain, between the coastal plateau and the shoreline. See location in Fig. 11.2C. AMS radiocarbon dates are in calendar years

further seaward. Similar deposits would apparently be the over-consolidated mud identified by Torres (1997) in the Amazon River mouth, in the bottom of a 17 m deep channel. The transgressive mud facies thins landward as it onlaps the Miocene substrate. Its absence on the inner half of the barrier-estuarine system could be related to non-deposition or erosion caused by a more intense tidal ravinement in a narrower incised valley, with stronger tidal current velocities and possibly a thinner deposit due to smaller accommodation space. This process was mentioned by Lessa et al. (1998) to explain the absence of transgressive mud facies in the landward half of Paranaguá Bay, Southern Brazil (Angulo et al., Chap. 5 this volume).

Erosion of the transgressive mud facies closer to the coastal cliffs might be ascribed to the establishment of tidal meanders, which laid down the tidal meandering facies over the fluvial sand and gravel facies. The contact between these facies may also represent the tidal ravinement surface. The presence of subtidal sand-flat and intertidal sand shoals deposited over transgressive mud facies (Fig. 11.16) indicates that an initially transgressive shallow intertidal sand sheet has continuously aggraded as the sea level rose. These facies (5 and 6) comprised the upper portion of the estuarine transgressive/aggradational deposit (Souza Filho et al. 2006). The presence of flaser bedding and wood fragments indicates that mangroves or muddy tidal flat existed close by. According to Masselink and Lessa (1995), bed

aggradation allows for a gradual transition from subtidal sandbar into inter-tidal shoal. A similar process is also inferred by Angulo et al. (Chap. 5 this volume) when describing the evolution of a beach-ridge plain over sub-tidal/intertidal sand bars in Baía de Paranaguá.

According to Dalrymple et al. (1992), estuaries in a mixed energy (tide plus wave) coast may be associated with short barrier islands. Besides the present barrier island, two older ones were identified on the coastal plain overlying intertidal shoals and underlying old mangrove mud. The first in-nermost barrier-island is associated with the Post-glacial sea level maxi-mum, dated at 5,913 cal yrs BP, when the coastline was situated some 12 km landward from the present one (Figs. 11.17a and 11.18a). The first barrier island emerged 10 km seaward of the active coastal cliffs (Fig. 11.17a), providing shelter for the growth of mangroves at its rear.

In accordance with Behling (2002), there is a general decrease of the pollen content in the mangrove deposits of the State of Pará between 5,600 and 3,600 cal yrs BP, suggesting a fall of sea level and a decrease of the forested area. This may also be the reason for the apparent existence of mangrove deposits only around the barrier island at 5,913 cal yrs BP and from 3,736 cal yrs BP onwards (Figs. 11.17b and 11.18b).

In the last 2000 years there has been a swift mangrove progradation in-ternal to the estuary, from the paleo-cliffs all the way to the 2nd barrier isl-and (Figs. 11.17c and 11.18c). It is initially suggested that such prograda-tion may have occurred in a more sheltered environment that came about with the development of a larger barrier island(s). According to Cohen et al. (2005), a fall of relative sea level up to 1 m below modern sea level has apparently occurred between 1,800 and 1,400 cal yrs BP. It was then followed by a gradual rise until 1,000 cal yrs BP, when sea level was rees-tablished to the present level. Figure 11.16 shows mangrove sediments progressively younger seaward, indicating that mudflat progradation was responsible for the restriction of the estuarine flow inside the present day channels.

The last sea-level rise episode has apparently started around 1,550 cal yrs BP, and is likely associated with the retrogradation of the 3rd genera-tion of barrier island, that is burying back-barrier mangrove deposits (Figs. 11.17d and 11.18d). Transgression is apparently an ongoing process, as in-dicated by washover fans and especially drowned (within the intertidal level) aeolian sand dunes at the rear of the barrier. Cohen et al. (2005), based on pollen analysis, also suggest that a recent sea level rise is pushing the mangrove forest to higher elevation zones.

11.5 The Amazon Mangrove Coast in Perspective

The northern coast of Brazil is characterized by macrotidal conditions, with average inner shelf spring-tidal ranges between 4 to 5 m. Macrotidal ranges (up to 6.3 m) are attained inside the estuaries too, and must have become a more recent phenomenon. This is because the estuaries were apparently short and very open close to the post-glacial sea level maximum, acquiring a geometry conducive to tidal amplification (long, well defined funnel shaped channels bordered by mangroves) only in the last 2,500 cal yrs BP.

Nevertheless, the coastal scenario is controlled by macrotidal processes, with wide estuary mouths and short and narrow barriers. For instance, similar barrier dimensions are observed in macrotidal settings in NW and NE Australia (Masselink and Lessa 1995; Lessa and Masselink 2006) and in SW Korea (Yang et al. 2006), where mean spring tide ranges vary from 5 to 7.3 m. Such strong tidal control on the coastal geomorphology of Northern Brazil is related to large estuarine volumes (large tidal prisms), ascribed more to the inherited coastal morphology, and coastal progradation, than to the tidal range. Numerous fluvial channels, whose topographic signature extends to the middle shelf, control the existence of large estuarine channels.

The presence of these channels landward of the paleocliff provided enough discharge (tidal and fluvial) to keep the estuaries opened at the end of the post-glacial marine transgression, when back-barrier embayments were at a minimum with the farthest coastal retrogradation. This is different to what is reported in other coastal settings regardless of the tidal range. In places such as Virginia-US (Filkenstein and Ferland 1987) and Korea (Yang et al. 2006), coastal recession and smaller estuarine volumes at the end of the Postglacial Marine Transgression closed off several estuaries.

A positive sediment budget must have been established at the end of the Postglacial Marine Transgression, and counteracted subsequent smaller rates of submergence of this coastal sector. Sand surplus allowed for different events of barrier growth and coastal progradation possibly associated with two transgressive pulses that followed small scale events of sea level fall. The geomorphology and morphostratigraphic information suggest that bar emergence, lateral spit growth and barrier roll over might have taken place at the same time all over the area. Given the highly dynamic innershelf, short spaced valleys and (apparently) large littoral drift rates, barriers might have been eroded at the same time others were being formed.
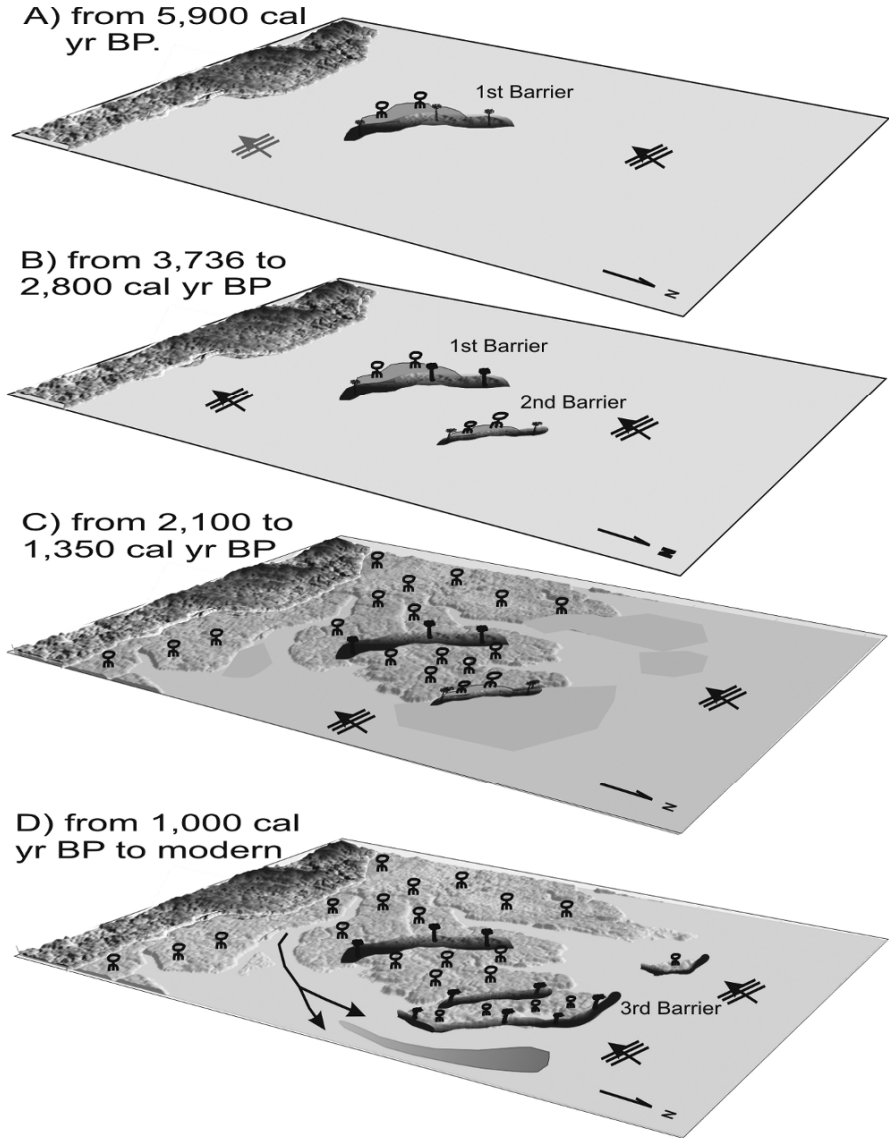
Fig. 11.17 Schematic evolution of the Caeté barrier estuary system based on remote sensing and field observations
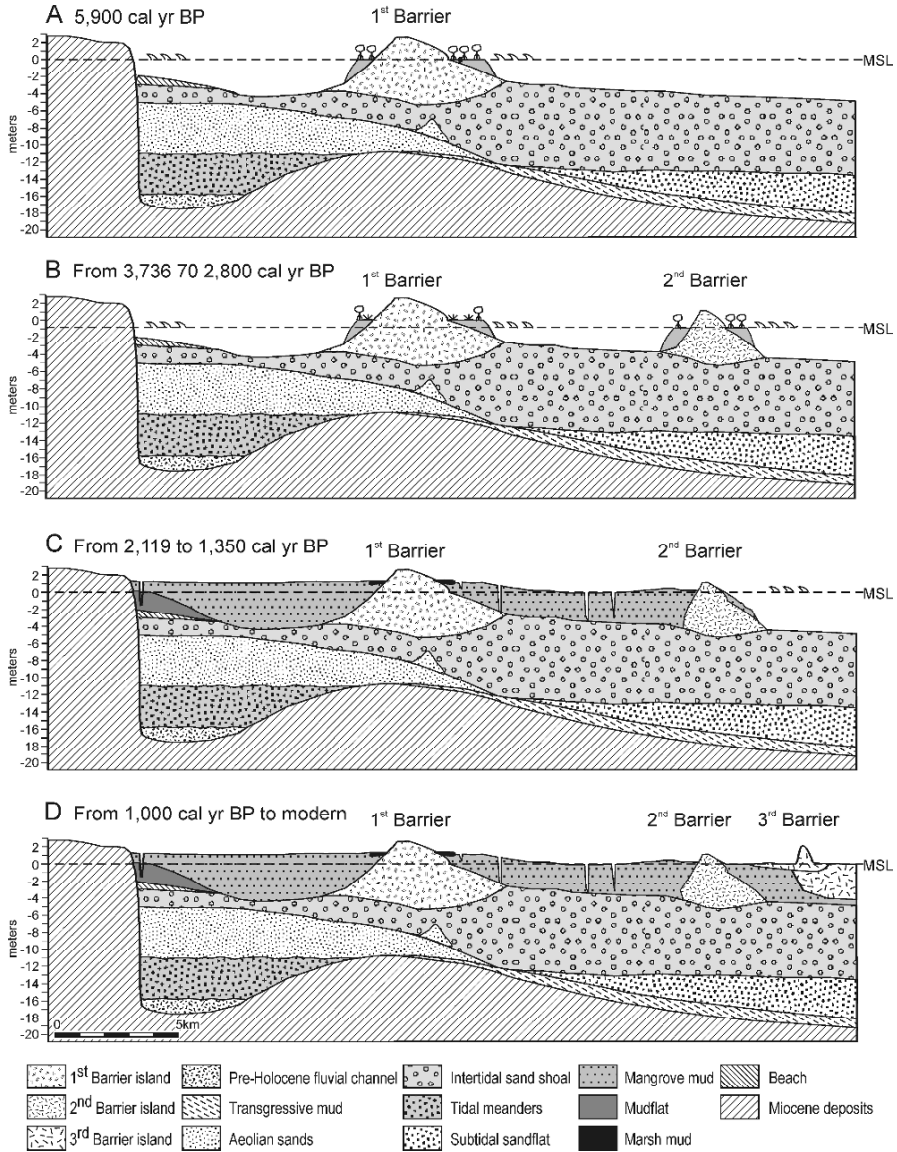
Fig. 11.18 Schematic model for the evolution of the shoreline in the Caeté barrier estuary system

The general aspect of the northern Pará coast is strikingly similar to that of the Sunderbans (India-Bangladesh), which is related to an abandoned part of the Ganges-Bramaputra river delta. In similarity to the Pará coast, numerous abandoned channel scars dominate the surface morphology of the abandoned delta plain (Coleman and Huh, 2007). The site is, however,

erosional, and possibly retrogradational, with fluvial streams now saline and tidally dominated (Coleman and Huh, 2007).

11.6 Conclusions

Contrary to the generally accepted idea that macrotidal settings (tidal range > 4 m) are not conducive to barrier formation (Davis and Hayes 1984), estuaries in this macrotidal coast are barred by sand bars and barriers.

The Caeté barrier estuary system evolved from a riverine environment into an intertidal muddy area accompanying the last eustatic sea-level rise. Deposition of the marine/estuarine facies has occurred in association with three generations of barrier islands, the last two generations apparently related to at least two small subsidence episodes in the last 3,000 years. The absence of mangrove deposits with ages between 5,913 and 2,800 cal yrs BP, as well as a general decrease of mangrove pollen in the whole region, suggests that a drop in sea level preceded the development of the second barrier-island. In the last 2,000 years, a relatively more stable sea level has apparently been conducive to the most significant progradation phase, when mangrove swamps prograded more than 20 km. Similar sedimentary processes might have occurred throughout the Eastern Pará coast, where mangrove plains and small barriers exist despite the varying size of the numerous estuaries and catchment areas.

References

Aranha LGF, Lima HP, Souza JMP, Makino RK (1990) Origem e evolução das bacias de Bragança-Viseu, São Luís e Ilha Nova. In: De Raja Gabaglia GP and Milani EJ (eds) Origem e evolução de bacias sedimentares. Petrobras,Rio de Janeiro, pp 221–233

Behling H, Cohen MCL, Lara RJ (2001) Studies on Holocene mangrove ecosystem dynamics of the Bragança Peninsula in north-eastern Pará, Brazil. Palaeogeog Palaeoclim Palaeoecol 167:225–242

Behling H (2002) Impact of the Holocene sea-level changes in coastal, eastern and Central Amazonia. Amazoniana XVII:41–52

Campos CWM, Ponte FC, Miura K (1974) Geology of the Brazilian continental margin. In: Burk CA and Drake CL (eds) The geology of continental margins. Springer-Verlag, Berlin, pp 447–461

Cavalcante SGH, Kjerfve B, Koppers BA, Diele K, Barreto RC (2005) Comportamento dos sedimentos em suspensão, temperatura e salinidade na região costeira adjacente a baía do Caeté. Annals of the 10° Congresso Brasileiro de Geoquímica, Porto de Galinhas

Cohen MCL, Souza Filho PWM, Lara RJ, Behling H, Angulo RJ (2005) A model of Holocene mangrove development and relative sea-level changes on the Braganca Peninsula (Northern Brazil). Wetlands Ecol Managem 13:433–443

Coleman JM, Huh OK (2007) Major world deltas: a perspective from space. Retrieved March 12, 2007, from Luisiana State University, Coastal Studies Institute Web site, http://www.geol.lsu.edu/WDD/PUBLICATIONS/C&Hnasa04/C&Hfinal04.htm

Costa JBS, Hasui Y, Bemerguy RL, Soares Jr. AV, Villegas JMC (2002) Tectonics and paleogeography of the Marajó Basin, northern Brazil. Anais Acad Bras Ciênc 74:519–531

CPRM (2001) Geologia, Tectônica e Recursos Minerais do Brasil. Sistema de Informações Geográficas – SIG – Mapas na escala 1:2.500.000. CPRM, Rio de Janeiro

Dalrymple RW, Zaitlin BA, Boyd R (1992) Estuary facies models: conceptual basis and stratigraphic implications. J Sedim Petrol 62:1130–1146

Davis RA, Hayes MO (1984) What is a wave-dominated coast? Mar Geol 60:313–329

DHN (1962) Departamento de Hidrografia e Navegação

Driskoll NW, Karner GD (1994) Flexural deformation due to Amazon fan loading: a feedback mechanism affecting sediment delivery to margins. Geology 22:1015–1018

Ferreira Jr. CRP, Costa JBS, Bermerguy RL, Hasui Y (1996) Neotectônica na área da Bacia de São Luís. Revista Geociências 15:185–208

Finkelstein K, Ferland MA (1987) Back-barreir response to sea-level rise, eastern shore of Virginia. In: Nummedal D, Pilkey OH, Howard JD (eds) Sea-level fluctuation and coastal evolution. SEPM, SP 41, pp 145–156

Gorayeb PSS, Gaudette HE, Moura CAV, Abreu FAM (1999) Geologia e geocronologia da Suíte Rosário, nordeste do Brasil, e sua contextualização geotectônica. Rev Bras Geoc 29:571–578

Gorini MA and Bryan GM (1976) The tectonic fabric of the Equatorial Atlantic and adjoining continental margins: Gulf of Guinea to northeastern Brazil. Anais Acad Bras Ciênc 48:101–119

Kjerfve B, Perillo GME, Gardner LR, Rine JM, Dias GTM, Mochel FR (2002) Morphodynamics of muddy environments along the Atlantic coasts of North and South America. In: Healy TR, Wang Y, Healy J-A (eds) Muddy Coasts of the World: processes, deposits and functions. Elsevier, Amsterdam, pp 219–239

Klein EL, Koppe JC, Moura CAV (2002) Geology and geochemistry of the Caxias gold deposits, and geochronology of the gold-hosting Caxias microtonalite, São Luís Craton, northern Brazil. J South Amer Earth Sci. 14:837–849

Koch B, Rullköter J, Lara RJ (2003) Evaluation of triterpenols and sterols as organic matter biomarkers in a mangrove ecosystem in Northern Brazil. Wetlands Ecol Manag 11:257–23

Lessa GC (2000) Morphodynamic controls on vertical and horizontal tides – field results from two macrotidal shallow estuaries: central Queensland, Australia. J Coastal Res 16:976–989

Lessa GC, Masselink G (2006) Evidence of a Mid-Holocene sea-level highstand from the sedimentary record of a macrotidal barrier and paleo-estuary system in northwestern Australia. J Coastal Res 22:100–112

Lessa GC, Meyers SD, Marone E (1998) Holocene stratigraphy in Paranaguá Bay estuary, south Brazil. J Sedim Res 68:1060–1076

Martins, ESF, Souza Filho PWM, Costa FR, Alves PJO (2007) Extração automatizada e caracterização da rede de drenagem e das bacias hidrográficas do nordeste do Pará ao noroeste do Maranhão a partir de imagens SRTM. Annals of the 13° Simpósio Brasileiro de Sensoriamento Remoto, Florianópolis

Masselink G and Lessa GC (1995) Barrier stratigraphy on the macro-tidal central Queensland coastline, Australia. J Coastal Res 11:454–477

Milliman JD (1979) Morphology and structure of Amazon upper continental margin. Amer Assoc Petrol Geologists Bull 63:934–950

Milliman JD, Barreto HT (1975) Relict magnesian calcite oolite and subsidence of Amazon Shelf. Sedimentology 22:37–145

Moraes BC, Costa JMN, Costa ACL, Costa MH (2005) Variação especial e temporal da precipitação no estado do Pará. Acta Amazônica 35:207–214

Rossetti DF (2001) Late Cenozoic sedimentary evolution in northeastern Pará, Brazil, within the context of sea level changes. J South Amer Earth Sci 14:77–89

Rossetti DF (2003) Delineating shallow Neogene deformation structures in northeastern Pará State using Ground Penetrating Radar. Anais Acad Bras Ciênc 75:235–248

Souza Filho PWM (2000) Tectonic control on the coastal zone geomorphology of the Northeastern Pará State.• Rev Bras Geoc 30:523–526

Souza Filho PWM (2005) Costa de Manguezais de Macromaré da Amazônia: Cenários Morfológicos, Mapeamento e Quantificação a partir de Dados de Sensores Remotos. Rev Bras Geof 23:427–435

Souza Filho PWM and El-Robrini M (1998) As variações do nível do mar e a estratigrafia de seqüências da Planície Costeira Bragantina – Nordeste do Pará, Brasil. Bol Mus Par Emílio Goeldi, Série Ciências Terra 10:45–78

Souza Filho PWM and El-Robrini M (2000) Coastal zone geomorphology of the Bragança area, Northeast of Amazon Region, Brazil. Rev Bras Geoc 30:518–522

Souza Filho PWM and Paradella WR (2005) Use of RADARSAT-1 Fine and Landsat-5 TM selective principal component analysis for geomorphological mapping in a macrotidal mangrove coast, Amazon Region. Can J Remote Sens 31:214–224

Souza Filho PWM, Cohen MCL, Lara RJ, Lessa GC, Koch, B, Behling H (2006) Holocene coastal evolution and facies model of the Bragança macrotidal flat on the Amazon Mangrove Coast, Northern Brazil. J Coastal Res SI 39:306–310

Souza Filho PWM, Tozzi HAM, El-Robrini M (2003) Geomorphology, land use and environmental hazard in Ajuruteua macrotidal sandy beach, northeastern, Pará, Brazil. J Coastal Res 35:580–589

Torres AM (1997) Sedimentology of the Amazon Mouth: North and South Channels, Brazil. PhD. thesis, University of Kiel

Yang BB, Dalrymple RW, Chun SS, Lee HJ (2006) Transgressive sedimentation and stratigraphic evolution of a wave-dominated macrotidal coast, western Korea. Mar Geol 235:35–48

Zembruscki SG, Gorini MA, Palma JJC, Costa MPA (1971) Fisiografia e distribuição dos sedimentos superficiais na Plataforma Continental Norte Brasileira. Bol Técnico Petrobras 14:127–155